The stored energy of cold work

Benzerga, A.A.; Brechet, Y.; Needleman, A.; van der Giessen, Erik

Link to publication in University of Groningen/UMCG research database

ELSEVIER

The stored energy of cold work: Predictions from discrete dislocation plasticity

A.A. Benzerga [a,*], Y. Bréchet [b], A. Needleman [c], E. Van der Giessen [d]

[a] *Department of Aerospace Engineering, Texas A&M University, College Station, TX 77843-3141, USA*
[b] *L.T.P.C.M., 1130 Rue de la Piscine, BP 75, Domaine Universitaire, 38402 Saint Martin D'Hères Cedex, France*
[c] *Division of Engineering, Brown University, Providence, RI 02912, USA*
[d] *Materials Science Center, University of Groningen, Nyenborgh 4, 9747 AG Groningen, The Netherlands*

Abstract

The stored energy of cold work is calculated for planar single crystals under tensile loading with plastic deformation occurring through dislocation glide. Superposition is used to represent the solution of boundary value problems in terms of the singular fields for discrete dislocations and image fields that enforce boundary conditions. Constitutive rules are used which account for the effects of line tension and three-dimensional dislocation interactions including dynamic junction formation. The stored energy is calculated both under load and after load removal and methods are devised to estimate the local plastic dissipation and to separate out the contribution of long-range stresses to the energy stored. Calculations are carried out up to imposed strains of 0.05–0.1 and the effects of strain level, dislocation structure and crystal orientation on the evolution of the stored energy are investigated. Although the flow stress and work hardening rate depend mainly on the dislocation density, the stored energy of cold work depends on details of the dislocation structure that forms, with any long-range dislocation stress field playing a significant role. The calculations exhibit a connection between the stored energy of cold work and the Bauschinger effect. It is also found that local energy storage values can differ substantially from the average value.
© 2005 Acta Materialia Inc. Published by Elsevier Ltd. All rights reserved.

Keywords: Dislocations; Metallic materials; Stored energy; Plastic work; Heat

1. Introduction

A portion of the mechanical energy expended in plastically deforming a solid is elastic and recoverable, while the remainder is the plastic work. Generally most, but not all, of the plastic working is converted into heating. The plastic work not converted into heat is the stored energy of cold work and, at least in crystalline metals, is the energy stored in an evolving defect structure.

The partitioning of the plastic working into heat generation and energy storage is of interest in a wide range of contexts. The defect structure in a ductile metal that has been deformed and unloaded is generally unstable so that, with time, it evolves so as to reduce the stored energy. For example, in polycrystalline metals the stored energy of cold work plays a significant role in driving recrystallization. Knowledge of the fraction converted to heat is needed for prediction of thermoplastic coupling phenomena such as the thermal softening behavior that promotes mechanical instabilities, e.g., necking and shear banding, and that affects the deformation mode occurring in machining and penetration. Also, since the stored energy is associated with an internal stress state, there is a direct connection between it and the Bauschinger effect. Because of the broad significance of the stored energy of cold work, there is a large literature aimed at its experimental determination, see, e.g., [1–6].

---

* Corresponding author. Tel.: +1 979 845 1602.
E-mail address: benzerga@aeromail.tamu.edu (A.A. Benzerga).

In general, the stored energy of cold work in metals arises from the evolution of a variety of defects including, for example, twins, stacking faults and grain or sub-grain boundaries as well as dislocations. The rate of accumulation of stored energy varies with the strain, strain-rate and stress state. Thus, in order to determine the evolution of the stored energy, the evolution of the defect structure needs to be predicted for the given loading conditions. Calculations of the stored energy, e.g., [7–10], are generally carried out within a continuum framework with internal variables used to characterize the defect evolution. Exceptions include [11] where a method is developed to calculate the stored energy from experimentally determined load–displacement responses and [12] where the stored energy is specified through a constitutive relation within the framework of multiple evolving natural configurations.

Here, we confine attention to circumstances where the only defects are dislocations and calculate the stored energy of cold work using discrete dislocation plasticity, e.g., [13–15]. Discrete dislocation plasticity calculations give the dislocation positions and, correspondingly, the spatial distributions of stress and strain at each time step so that, within a purely mechanical framework, the stored energy is obtained from the difference between the internal energy associated with the dislocation structure in the current state and that in the initial state. Since the work input is readily determined at any stage of the loading history, the portion of the plastic work available for heat generation is simply the input mechanical work minus the stored energy of cold work. Thus, discrete dislocation plasticity provides a framework for the direct calculation of the stored energy of cold work.

The methodology is illustrated for single crystals subject to tensile loading. The calculations are carried out for planar model crystals using physically based dislocation constitutive rules that incorporate key three-dimensional effects such as dynamic junction formation and destruction, dynamic source production and line tension [15]. The stored energy is calculated in both the loaded state and the unloaded state. The effects of strain level, dislocation structure and crystal orientation on the evolution of the stored energy are explored.

2. Problem formulation and analysis

Calculations are carried out assuming small strains and rotations for a planar model fcc crystal having dimensions $2l \times 2h$, subject to plane strain uniaxial tension in the x_1–x_2 plane, Fig. 1(a). Deformation is imposed by prescribing a uniform displacement $u_1 = \pm U$ along $x_1 = \pm l$, where the shear traction vanishes. The lateral surfaces at $x_2 = \pm h$ are traction free. There are two slip systems oriented at $\pm|\varphi_0|$ with φ_0 the angle between the tensile x_1-axis and the $[1\bar{1}2]$ direction; see
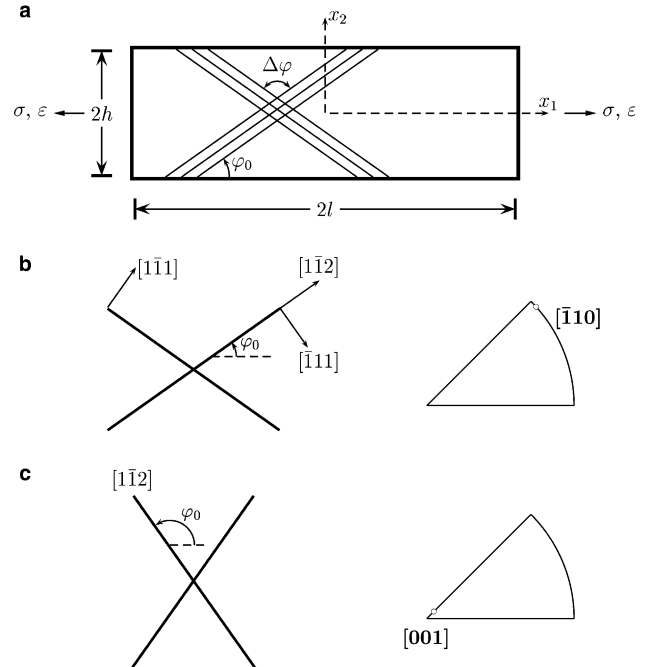

Fig. 1. Geometry of the tension problem for a planar model fcc crystal oriented for double slip. (a) Definition of the crystal orientation with $\Delta\varphi = 109.5°$ and φ_0 referring to the angle between the loading x_1-axis and the $[1\bar{1}2]$ direction. (b) Configuration for $[\bar{1}10]$ tension with $\varphi_0 = 35.25°$. (c) Configuration for $[001]$ tension with $\varphi_0 = 125.25°$.

Fig. 1. The orientations analyzed are: (i) near $[\bar{1}10]$ as in [15] with $\varphi_0 = 35.25°$; and (ii) near $[001]$ with $\varphi_0 = 125.25°$.

The two-dimensional, plane strain discrete dislocation formulation of [13] is used together with its recent extension [15] to incorporate some key aspects of three-dimensional dislocation interactions and line tension. Plastic flow arises from the glide of edge dislocations, modeled as line singularities in an elastic continuum, on specified slip planes. At time t, the body is in equilibrium with the applied loads and displacements, and the position of each dislocation in the body is known. An increment of loading is applied and at each time step obtaining the solution involves: (i) determining the displacement and stress fields for the current dislocation arrangement; (ii) determining the forces on the dislocations; (iii) determining the rate of change of the dislocation structure.

The glide component of the Peach–Koehler force, f^i, on dislocation i is given by

$$f^i = \mathbf{m}^i \cdot \left(\hat{\boldsymbol{\sigma}} + \sum_{j \neq i} \boldsymbol{\sigma}^j \right) \cdot \mathbf{b}^i, \tag{1}$$

where $\boldsymbol{\sigma}^j$ is the stress field of dislocation j, in its current configuration, but in an infinite homogeneous medium [16], $\hat{\boldsymbol{\sigma}}$ is the image stress determined from a finite element computation, $\mathbf{m}^i$ is the slip plane normal and $\mathbf{b}^i$ the Burgers vector having magnitude $|b^i| = b$.

The formulation of the constitutive rules follows that in [15] where the physical background for the rules is given along with additional references. A key event for the creation of dynamic obstacles and sources is junction formation. This is taken to occur when two dislocations gliding on intersecting slip planes approach within a specified distance $d^{\star}$ from the intersection point of the slip plane traces. Two types of junctions can form: one, referred to as an obstacle, can be destroyed by the local stress exceeding a specified value; the other, referred to as an anchoring point, can only be destroyed by annihilation of one of the dislocations forming the junction. Annihilation occurs between coplanar dislocations having opposite signed Burgers vector when they are within a prescribed critical distance L_e. Whether a junction acts as an anchoring point or an obstacle is treated as a statistical event. The probability of forming an anchoring point has the prescribed value p.

Source operation is a process involving two junctions on the same slip plane, one of which must be an anchoring point. In plane strain, a dislocation dipole is nucleated at source I if the value of the Peach–Koehler force at the junction exceeds the value $\tau^I_{\text{nuc}}b$, during a time t^I_{nuc}. The nucleation stress is taken to be given by

$$\tau^I_{\text{nuc}} = \beta \frac{\mu b}{\mathscr{S}^I}, \tag{2}$$

where $\mathscr{S}^I$ is the distance to the nearest junction in any of the two intersecting planes and β a factor of order unity. The nucleation time is given by

$$t^I_{\text{nuc}} = \gamma \frac{\mathscr{S}^I}{|\tau^I|b}, \tag{3}$$

where τ^I is the current resolved shear stress at the location of junction I and γ is a material characteristic factor taken here as a constant. Note that longer segments are activated at lower stresses, but nucleation takes a longer time. The nucleated dislocations form a dipole and are located on either side of the activated segment.

Obstacle I is destroyed if the Peach–Koehler force acting on either dislocation comprising the junction attains or exceeds the breaking force $\tau^I_{\text{brk}}b$ specified by

$$\tau^I_{\text{brk}} = \beta \frac{\mu b}{\mathscr{S}^I} \tag{4}$$

with β and $\mathscr{S}^I$ as above. When the junction is destroyed, the dislocations forming the junction, as well as those pinned at the junction, are released and free to glide on their respective slip planes.

In the calculations, two possibilities are considered: (i) junctions are not destroyed by annihilation so that an obstacle I can only be destroyed if τ^I_{brk} is reached or exceeded but anchoring points cannot be destroyed; and (ii) junctions, either obstacles or anchoring points, can be destroyed by annihilation of one of the two dislocations forming it.

To represent the energy cost associated with loop expansion in two dimensions, a configurational force of magnitude $|\mathscr{L}^i b^i|$ is introduced that points from one dislocation, i, comprising the dipole toward the other and $\mathscr{L}^i$ is written as

$$\mathscr{L}^i = -\alpha \frac{\mu |b^i|}{\mathscr{S}^i_{\text{d}}}, \tag{5}$$

where α is a proportionality factor, hereafter called the line tension parameter, and $\mathscr{S}^i_{\text{d}}$ is the algebraic distance between the dislocations, members of the same dipole, so that the sign of $\mathscr{L}^i$ depends on the sign of $\mathscr{S}^i_{\text{d}}$. Note that $\mathscr{L}^i$ has units of a stress and that the work of the restoring force, $\mathscr{L}^i b^i$, is the additional energy per unit length $\alpha \mu b^2$ [15,17].

The dislocation glide relation is written in the form

$$B v^i = (\tau^i + \mathscr{L}^i) b^i \tag{6}$$

with v^i the glide velocity of dislocation i and B the drag coefficient.

There are no mobile dislocations initially but a number of initial point sources and point obstacles, randomly located on the slip planes, is specified. These initial sources and obstacles do not evolve with the deformation history so that their number is fixed throughout a calculation.

Each initial source nucleates a dislocation dipole when the resolved shear stress at the location of source i, exceeds the value τ^i_{0n} for a prescribed time t_{0n}. The size of the generated loop, L^i_{0n}, which corresponds to the dipole separation, is inversely proportional to the nucleation stress [13]. Dislocations can get pinned at the initial point obstacles and are released once the Peach–Koehler force at the location of the obstacle attains the value $\tau_{\text{obs}}b$.

3. Calculation of the stored energy

Attention is restricted to quasi-static deformations in the context of a purely mechanical theory, so that the power balance can be written as

$$\int_S \mathbf{t} \cdot \dot{\mathbf{u}} \, dS = \int_V \dot{\phi} \, dV + \int_V \zeta \, dV, \tag{7}$$

where the term on the left-hand side is the power expended by the external loads in the absence of body forces, $\dot{\phi}$ is the rate of change of the free energy density, ζ is the dissipation rate per unit volume, and V and S are, respectively, the volume and surface of the sample. In a more general thermodynamic framework, Eq. (7) would contain additional heat flux and entropy production terms but the purely mechanical calculations here provide no basis for including these contributions.

For the materials under consideration,

$$\Phi = \int_V \phi \, \mathrm{d}V = \frac{1}{2} \int_V \boldsymbol{\sigma} : \boldsymbol{\varepsilon} \, \mathrm{d}V \tag{8}$$

is the free energy of the sample, with

$$\boldsymbol{\sigma} = \mathbf{L} : \boldsymbol{\varepsilon}, \tag{9}$$

where $\mathbf{L}$ is the tensor of elastic moduli. The free energy density ϕ is a state function of the lattice strain $\boldsymbol{\varepsilon}$, so that, when dislocations are present in V, the free energy depends on the dislocation positions.

Using superposition, e.g., $\boldsymbol{\sigma} = \tilde{\boldsymbol{\sigma}} + \hat{\boldsymbol{\sigma}}$ with the (~)-fields being the superposition of individual dislocation fields in an infinite medium and the (^)-fields image fields that enforce the boundary conditions, Eq. (8) is written as

$$\Phi = \frac{1}{2} \int_V (\tilde{\boldsymbol{\sigma}} + \hat{\boldsymbol{\sigma}}) : (\tilde{\boldsymbol{\varepsilon}} + \hat{\boldsymbol{\varepsilon}}) \, \mathrm{d}V. \tag{10}$$

Since the stress and strain fields associated with the individual dislocations have a $1/r$ singularity, the value of Φ is not finite. We exclude a region around each dislocation core and attribute a finite energy to this region which is therefore proportional to the dislocation line length. Explicitly, from [18] and [13] with the core energy added,

$$
\begin{aligned}
\Phi = {}& \frac{1}{2} \int_V \hat{\boldsymbol{\sigma}} : \hat{\boldsymbol{\varepsilon}} \, \mathrm{d}V + \frac{1}{2} \int_V (\hat{\boldsymbol{\sigma}} : \tilde{\boldsymbol{\varepsilon}} + \tilde{\boldsymbol{\sigma}} : \hat{\boldsymbol{\varepsilon}}) \, \mathrm{d}V \\
&+ \frac{1}{2} \sum_{j \neq k} \sum \int_V \boldsymbol{\sigma}^j : \boldsymbol{\varepsilon}^k \, \mathrm{d}V \\
&+ \underbrace{\left\{ \sum_i \left[\frac{1}{2} \int_{\hat{V}^i} \boldsymbol{\sigma}^i : \boldsymbol{\varepsilon}^i \, \mathrm{d}V + \frac{1}{2} \int_{C^i} \mathbf{t}^i \cdot \mathbf{u}^i \, \mathrm{d}S \right] + E_c^i \right\}}_{E_1^s},
\end{aligned}
\tag{11}
$$

where the sums are over all dislocations in V, C^i is the surface of the excluded region around the core of dislocation i and $\hat{V}^i = V \setminus V^i$, with V^i the excluded core volume. The term in curly brackets in Eq. (11) gives the self-energy and core energy contributions which together are termed the line energy, E_1^s. The remaining terms in Eq. (11) include the dislocation interaction energy, the energy of the image field and the interaction energy between the image field and the individual dislocation fields. In a two-dimensional plane strain formulation, the edge dislocation dipoles are regarded as a planar cut through a dislocation loop. The separation of the dislocation dipoles then corresponds to loop expansion. The term E_c^i is a constitutive addition to account for the energy associated with the corresponding core expansion, which is not accounted for in the elastic representation of dislocations. The calculation of E_1^s is described in the Appendix.

Next consider two stages in a program of loading: one at time t_1, the other at time t_2 and define,

$$\mathcal{D} = \int_V \zeta \, \mathrm{d}V, \quad \dot{\mathcal{W}} = \int_S \mathbf{t} \cdot \dot{\mathbf{u}} \, \mathrm{d}S. \tag{12}$$

Integrating Eq. (7) gives

$$\int_{t_1}^{t_2} \dot{\mathcal{W}} \, \mathrm{d}t + \Phi(t_1) - \Phi(t_2) = \int_{t_1}^{t_2} \mathcal{D} \, \mathrm{d}t. \tag{13}$$

The free energy change, $\Phi(t_2) - \Phi(t_1)$, represents the energy stored in the sample. It is approximately equal to the internal energy change at ordinary and low temperatures, because the entropy contribution is negligible [19].

Here, we consider tension of the plane strain strip of Fig. 1 for which, per unit thickness,

$$\mathcal{W} = A \int_{t_1}^{t_2} \sigma \dot{\varepsilon} \, \mathrm{d}t, \tag{14}$$

where σ and $\dot{\varepsilon}$ are the overall axial stress and strain rate, and $A = (2h)(2l)$ is the in-plane area of the specimen. Thus, $\mathcal{W}/A$ is the area under the overall stress-strain curve between t_1 and t_2. Since the overall response is an outcome of the boundary value problem solution, and $\Phi(t_1)$ and $\Phi(t_2)$ can be calculated directly from Eq. (11), the dissipated energy $\int_{t_1}^{t_2} \mathcal{D} \, \mathrm{d}t$ is readily determined by Eq. (13).

Now, consider loading from an initial ($t_1 = 0$) stress-free state so that $\Phi(0) = 0$. Then,

$$\int_0^{t_2} \mathcal{D} \, \mathrm{d}t = \int_0^{t_2} \dot{\mathcal{W}} \, \mathrm{d}t - \Phi(t_2). \tag{15}$$

Suppose, in addition, that the state at t_2 corresponds to an unloaded state after some program of loading, i.e., when the strip is traction free on all external surfaces. Then $\Phi(t_2)$ is the free energy associated with a residual self-equilibrated stress state. If dislocations remain in the body in the unloaded state $\Phi(t_2) > 0$ and the dissipation will be less than the area under the stress strain curve (Φ is strictly positive unless $\boldsymbol{\sigma}$ vanishes everywhere).

In the loaded state, there is a contribution to Φ from the work of the loads (i.e., the macroscopic elastic strain energy) in addition to the energy associated with the dislocation structure. For plane strain tension, the elastic energy associated with the applied stress σ is

$$\mathcal{W}^e = \frac{A}{2\bar{E}} \sigma^2, \tag{16}$$

where $\bar{E}$ is the plane strain tensile modulus, $\bar{E} = E/(1 - v^2)$, with E Young's modulus and v Poisson's ratio. From Eqs. (14) and (16), the plastic work, $\mathcal{W}^p$, is

$$\mathcal{W}^p = \mathcal{W} - \mathcal{W}^e. \tag{17}$$

The stored energy is defined as

$$E^s = \Phi(t_2) - \mathcal{W}^e. \tag{18}$$

When the specimen is unloaded, say at $t = t_u$, $\mathscr{W}^e(t_u) = 0$ so that the stored energy in the unloaded state, E_u^s is simply

$$E_u^s = \Phi(t_u). \tag{19}$$

In general, the stored energy, E^s, in the loaded state ($\sigma \neq 0$) is not equal to its value, E_u^s, after removal of the loads ($\sigma = 0$). Thus, part of the energy stored in the dislocation structure may be recovered on unloading due to a rearrangement of the dislocation structure. At any stage of loading, E^s can be calculated from Eq. (18) with Φ computed from Eq. (11) while the total work of deformation, $\mathscr{W}$, is computed from Eq. (14).

In addition to the overall stored energy, we also present spatial distributions of stored energy and dissipation rate. Analogous to Eq. (10), the local rate of change of the specific stored energy is written as

$$\dot{\phi} = \boldsymbol{\sigma} : \dot{\boldsymbol{\varepsilon}} = (\tilde{\boldsymbol{\sigma}} + \hat{\boldsymbol{\sigma}}) : \left(\dot{\tilde{\boldsymbol{\varepsilon}}} + \dot{\hat{\boldsymbol{\varepsilon}}} \right), \tag{20}$$

except at points within the core radius of a dislocation. Since in discrete dislocation plasticity, the plastic part of the deformation is associated with the evolution of displacement jumps across the slip planes, the displacement gradient field involves delta functions which need to be accounted for to compute the plastic dissipation directly. Here, to simplify the calculation, an approximation is used to calculate the plastic dissipation. A smooth strain rate field, $\dot{\boldsymbol{\varepsilon}}^s$, is introduced in each finite element that is computed by differentiating the total displacement rate field $\dot{\mathbf{u}}$ in that element using the finite element shape functions. Then, within an element, $\boldsymbol{\sigma} : \dot{\boldsymbol{\varepsilon}}^s$ is the local working and ζ is calculated from

$$\zeta = \boldsymbol{\sigma} : \dot{\boldsymbol{\varepsilon}}^s - \dot{\phi} = \dot{w} - \dot{\phi}. \tag{21}$$

4. Results

Attention is mainly focused on three sets of parameters, which were also considered in [15] and denoted by crystal A, crystal B and crystal C. For all three crystals,

$v = 0.3$, $E = 70$ GPa, $b = 0.25$ nm and $B = 10^{-4}$ Pa s. The annihilation distance is taken to be $L_e = 6b = 1.5$ nm, the critical distance for junction formation is $d^{\star} = 6b$ and the core cut-off radius is $2b$. The initial, static obstacles have a uniform strength, while the strengths of the initial, static sources are taken to follow a Gaussian distribution. Initially unsymmetric slip is considered by assigning the initial sources of the two slip systems unequal mean strengths. Reference parameters for each crystal analyzed are given in Table 1. The motivation for the range of parameters used here is discussed in [15]. In particular, a representative range for α is 0.2–0.4; see e.g. [20]. The effect of the line tension parameter α, Eq. (5), on the evolution of the dislocation structure is analyzed for crystal A. For crystals B and C α is taken equal to zero in order to focus attention on the effects of dynamic junctions and sources. However, when calculations of the dislocation evolution are carried out with $\alpha = 0$ in Eq. (5) some results are shown with $\alpha = 0.2$ in the expression for E_i^s given in Eq. (29) of the Appendix in order to indicate the relative contributions of the interaction energy and the line energy for a given dislocation configuration.

Some key features exhibited by the results in [15] for the same crystals analyzed here are: (i) a transition from stage I to stage II hardening, initiated by an increase in the number of dynamic junctions and in dislocation source activity; (ii) scaling of the flow strength in stage II with the square root of the dislocation density; and (iii) the formation of dislocation structures that refine with increasing deformation. The value of the pre-factor, a, in the expression

$$\mathscr{T} = a\mu b \sqrt{\rho} \tag{22}$$

for the flow stress $\mathscr{T}$ was found to fall within the range 0.4–0.5, in keeping with experiments (see [15] and references therein). The value of the computed work hardening rate and the rate at which dislocation structures form depended sensitively on whether or not anchoring points could be destroyed by annihilation. The stage II hardening rate was as low as $2 \times 10^{-3}\mu$ when destruction by annihilation was allowed, and as high as $2 \times 10^{-2}\mu$ if

Table 1
Properties of the three crystals analyzed

Crystal	Orientation	Size $2l \times 2h$ (µm²)	d	Static initial sources				Static initial obstacles		Dynamic junctions			
				ρ_0 (m⁻²)	$\bar{\tau}_{0n}$ (MPa)	SD (MPa)	t_{0n} (ns)	ρ_{obs} (m⁻²)	τ_{obs} (MPa)	p	α	β	γ (Pa s)
A	$[\bar{1}10]$S	12×4	$100b$	1.2×10^{13}	50	15	10	1.8×10^{13}	150	0.05	0.4	1	0.2
A	$[\bar{1}10]$S	12×4	$100b$	1.2×10^{13}	50	15	10	1.8×10^{13}	150	0.05	0	1	0.2
B	$[\bar{1}10]$U	6×2	$50b$	4.9×10^{13}	50$^{(1)}$	10$^{(1)}$	10	4.9×10^{13}	150	0.05	0	1	0.1
B	$[\bar{1}10]$S	6×2	$50b$	4.9×10^{13}	50	10	10	4.9×10^{13}	150	0.05	0	1	0.1
B	$[001]$S	6×2	$50b$	10×10^{13}	50	10	10	10×10^{13}	150	0.05	0	1	0.1
C	$[\bar{1}10]$U	6×2	$25b$	4.9×10^{13}	75$^{(2)}$	15$^{(2)}$	10	9.7×10^{13}	150	0.02	0	5	0.1

The labels S and U refer to initially symmetric slip and initially unsymmetric slip, respectively. (^{1}) These values pertain to the slip system at φ_0; the slip system at $\varphi_0 + \Delta\varphi$ has $\bar{\tau}_{0n} = 75$ MPa and a standard deviation of 15 MPa. (^{2}) These values pertain to the slip system at φ_0; the slip system at $\varphi_0 + \Delta\varphi$ has $\bar{\tau}_{0n} = 50$ MPa and a standard deviation of 15 MPa. Some values given in Ref. [15] for ρ_0 and ρ_{obs} were not correct.

not. The higher work hardening rate was associated with dislocation structure formation at smaller strains. In the results presented here for crystals A and B dynamic obstacles can only be destroyed if the obstacle strength is attained, while for crystal C dynamic obstacles also can be destroyed by annihilation of one of the dislocations forming the junction.

Here, unloading as well as loading calculations are carried out and the stored energy is computed both under load and at zero load. All calculations are carried out with $|\dot{U}| = 2 \times 10^3 \ \mu\mathrm{m} \ \mathrm{s}^{-1}$ so that the strain rate is of the order of $10^2 \ \mathrm{s}^{-1}$. The total work of deformation, $\mathscr{W}$ in Eq. (14), the plastic work, $\mathscr{W}^{\mathrm{p}}$ in Eq. (17), the stored energy in the loaded state, E^{s} in Eq. (18), and the stored energy in the unloaded state, $E^{\mathrm{s}}_{\mathrm{u}}$ in Eq. (19), are computed per unit thickness. Two energy storage ratios are of interest: (i) $E^{\mathrm{s}}_{\mathrm{u}}/\mathscr{W}$ for comparison with most experiments, e.g. [1,3,4]; and (ii) $E^{\mathrm{s}}/\mathscr{W}^{\mathrm{p}}$. The latter will be compared to the rate of energy storage, $\dot{E}^{\mathrm{s}}/\dot{\mathscr{W}}^{\mathrm{p}}$, which is measured in dynamic experiments [2,5,6] and often enters formulations of thermomechanical constitutive relations.

The applied strain, ε, the overall plastic strain, ε^{p}, and the average tensile stress, σ, are given by (see Fig. 1(a)),

$$\varepsilon = \frac{U}{\ell}, \quad \varepsilon^{\mathrm{p}} = \varepsilon - \frac{\sigma}{\bar{E}}, \quad \sigma = \frac{1}{2h} \int_{-h}^{+h} \sigma_{11}(\pm\ell, x_2) \, \mathrm{d}x_2.$$

(23)

Results are first presented for crystal C with initially unsymmetric slip which has a relatively low, but representative, hardening rate. In this case, a distinct dislocation pattern does not form over the strain range computed. Then, results are presented for crystal B with initially unsymmetric slip and for crystal A with initially symmetric slip using parameter values that give rise to increased dislocation storage leading to high hardening and dislocation patterning. This permits the effect of a more fully developed dislocation structure on the energy storage to be investigated. For crystal B, the evolution of the energy storage for the configurations with initially symmetric and initially unsymmetric slip are then compared. Finally, again for crystal B (with initially symmetric slip), the energy storage evolution for the two orientations in Fig. 1 is considered.

4.1. Low dislocation storage

Fig. 2 shows curves of σ versus ε^{p} for crystal C with initially unsymmetric slip. In this crystal, an obstacle can be destroyed by annihilation of one of the two dislocations forming it as well as by its strength being reached. Calculations unloading to $\sigma = 0$ are carried out at strain intervals of about 0.01. The unloading response remains essentially elastic for all pre-strains. The dislocation density varies only slightly during unloading (the evolution of the dislocation density
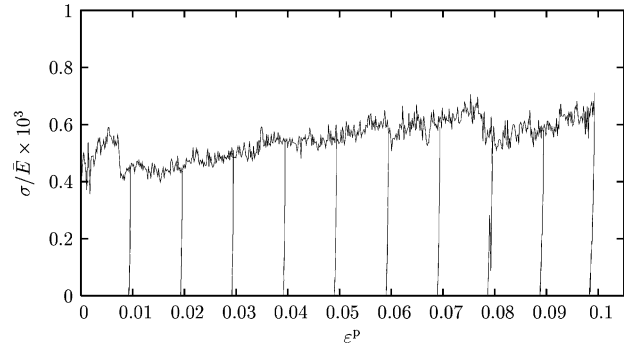

Fig. 2. Stress, σ, normalized by the plane strain tensile modulus, $\bar{E}$, versus plastic strain, ε^{p} for crystal C in tension and with unloading to $\sigma = 0$ from several strain levels (slip is initially unsymmetric).

during loading is shown in Fig. 11 of [15]), consistent with the absence of significant reverse plasticity.

Fig. 3(a) shows the evolution of the stored energy normalized by the plastic work, $E^{\mathrm{s}}/\mathscr{W}^{\mathrm{p}}$, while Fig. 3(b) shows the evolution of the stored energy after unloading normalized by the total work of deformation, $E^{\mathrm{s}}_{\mathrm{u}}/\mathscr{W}$. The calculation of the dislocation evolution is carried out with $\alpha = 0$ in Eq. (5) but results are shown both with $\alpha = 0$ and with $\alpha = 0.2$ in Eq. (29) of the Appendix. Thus the dotted line ($\alpha = 0$) shows only the interaction energy while the solid line ($\alpha = 0.2$) includes
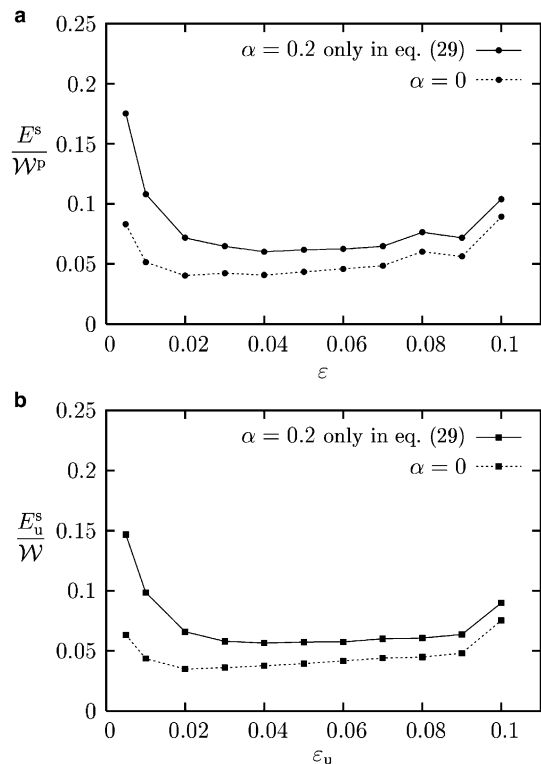

Fig. 3. Evolution of the energy storage with strain for crystal C. (a) Ratio of stored energy, E^{s}, to plastic work, $\mathscr{W}^{\mathrm{p}}$, versus imposed strain, ε. (b) Ratio of stored energy after unloading, $E^{\mathrm{s}}_{\mathrm{u}}$, to the total work of deformation, $\mathscr{W}$, versus the strain ε_{u} at the beginning of unloading.

the line energy contribution from Eq. (29). The plastic work, $\mathcal{W}^p$, and the total work, $\mathcal{W}$, essentially coincide so that any difference between the ratios $E^s/\mathcal{W}^p$ and $E_u^s/\mathcal{W}$ in Fig. 3 is due to the difference between E^s and E_u^s, which is small since the dislocation structure does not change much during unloading. In both Figs. 3(a) and (b), after an initial transient, the energy stored in the dislocation structure represents less than 8% of $\mathcal{W}$ (Fig. 3(a)) and $\mathcal{W}^p$ (Fig. 3(b)) up to $\varepsilon \approx 0.09$. The energy storage ratios decrease at first ($\varepsilon < 0.02$) and then slowly increase. With the line tension contribution accounted for in computing E^s and E_u^s (solid lines) the energy storage ratios are higher, as expected. The effect of line tension is greater at small strains because with a low dislocation density the elastic interaction energy is small so that the line energy contribution is more significant. This low hardening crystal has low energy storage ratios, an absence of reverse plasticity on unloading, low dislocation densities and no dislocation organization over the range of strain computed.

4.2. High dislocation storage

We now consider calculations giving a high hardening rate by letting the obstacles be destroyed only if the obstacle strength is attained. This results in an increase in the number of dislocation sources which leads to a more rapidly increasing dislocation density. As a consequence, dislocation patterning is seen [15]. The effect of this increased dislocation activity and organization on the evolution of the stored energy is considered in this section.

Figs. 4 and 5 show results for crystal B, with initially unsymmetric slip, both with line tension accounted for in computing the energy stored ($\alpha = 0.2$ in Eq. (29) but $\alpha = 0$ in Eq. (5)) and with line tension neglected ($\alpha = 0$ in both Eqs. (5) and (29)). In Fig. 4, which shows the computed curves of σ versus ε^p, there is a strong Bauschinger effect with reverse yielding occurring while $\sigma > 0$. The magnitude of the Bauschinger effect increases with increasing strain. On unloading from $\varepsilon^p > 0.02$, the dislocation density increases at a rate roughly equal to the rate of increase during loading.

The evolution of the normalized stored energy under load, $E^s/\mathcal{W}^p$, and in the unloaded state, $E_u^s/\mathcal{W}$, is shown in Figs. 5(a) and (b), respectively. Both ratios increase with strain at a much faster rate than for the low dislocation storage case in Section 4.1, Fig. 3. Even with $\alpha = 0$, $E^s/\mathcal{W}^p$ and $E_u^s/\mathcal{W}$ are above 15% at $\varepsilon_u = 0.05$; by contrast, at $\varepsilon_u = 0.05$ in Fig. 3 both $E^s/\mathcal{W}^p$ and $E_u^s/\mathcal{W}$ are less than 5%. Moreover, the difference between $E^s/\mathcal{W}^p$ and $E_u^s/\mathcal{W}$ is larger than in Fig. 3 since the dislocation structure changes significantly during unloading. Fig. 5 also shows that with only static sources and obstacles (denoted by SI) the energy storage ratios in the loaded and unloaded states, $E^s/\mathcal{W}^p$ and
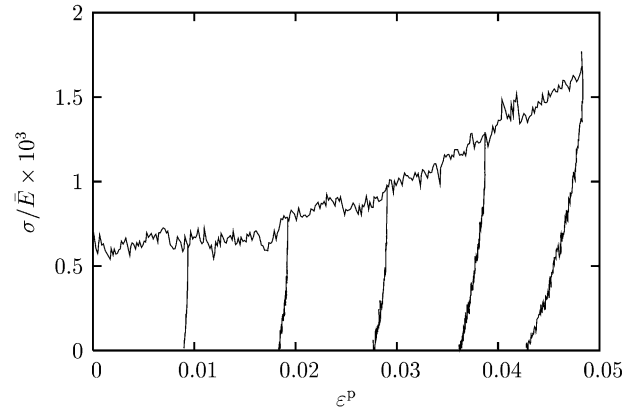

Fig. 4. Stress, σ, normalized by the plane strain tensile modulus, $\bar{E}$, versus plastic strain, ε^p, for crystal B in tension and with unloading to $\sigma = 0$ from several strain levels (slip is initially unsymmetric).
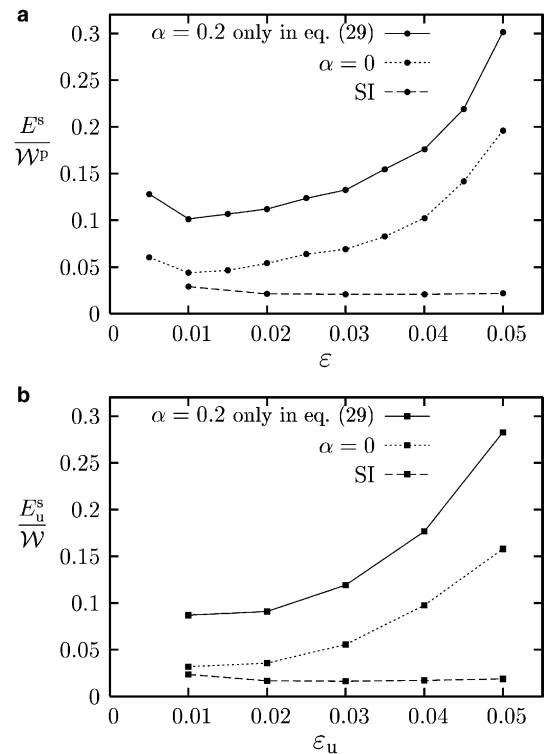

Fig. 5. Evolution of the energy storage with strain for crystal B. (a) Ratio of stored energy, E^s, to plastic work, $\mathcal{W}^p$, versus imposed strain, ε. (b) Ratio of stored energy after unloading, E_u^s, to the total work of deformation, $\mathcal{W}$, versus the strain ε_u at the beginning of unloading. The response with only static sources and obstacles is denoted by SI.

$E_u^s/\mathcal{W}$, are less than 2% over the entire strain range computed. This behavior is associated with the absence of hardening mechanisms when only static sources and obstacles are used, which leads to saturation of the dislocation density to a value one order of magnitude smaller than that reached at $\varepsilon \approx 0.035$ in the simulations allowing for dynamic junctions and source production.

The results for crystal A are shown in Fig. 6. In this case slip is initially symmetric so that no stage I occurs and the onset of stage II is concurrent with yielding. Here, a computation is carried out with $\alpha = 0.4$ in both Eqs. (5) and (29) so that the effect of line tension on the evolution of the dislocation structure is seen. Without line tension accounted for ($\alpha = 0$) the average work-hardening rate is nearly the same as with $\alpha = 0.4$ but there are strain intervals around 0.005 and 0.025 where the work hardening rate with $\alpha = 0$ is significantly reduced so that the flow strength falls below that with $\alpha = 0.4$.

Fig. 7 shows the effect of line tension on the evolution of the stored energy for crystal A. In Fig. 7(a), results are also shown where $\alpha = 0$ in Eq. (5) but the line tension contribution in Eq. (29) is included. A comparison of this curve with those for $\alpha = 0.4$ (in both Eqs. (5) and (29)) and $\alpha = 0$ shows that accounting for line tension in the evolution of the dislocation structure mainly affects the stored energy in the early stages of deformation but for $\varepsilon \approx 0.035$ and greater, accounting for line tension just adds a constant value to $E^s/\mathscr{W}^p$ and $E_u^s/\mathscr{W}$. In Fig. 7(b), the difference in stored energy in the unloaded state between the calculations with $\alpha = 0$ and with line tension accounted for ($\alpha = 0.4$) increases with increasing strain indicating an increased difference in the internal stress state.

It is worth noting that the ratios $E^s/\mathscr{W}^p$ or $E_u^s/\mathscr{W}$ vary more slowly for crystal A than for crystal B (Fig. 5) even though the work hardening rates are similar. In addition to the statistical effect of different initial conditions, the relatively small variations of $E^s/\mathscr{W}^p$ and $E_u^s/\mathscr{W}$ with applied strain in crystal A may be associated with a higher degree of dislocation organization, as was noted in [15]. Also, Fig. 7(a) shows that $E^s/\mathscr{W}^p$ tends to decrease at strains larger than 0.04. This trend did not occur for crystal B where stage II was shorter.
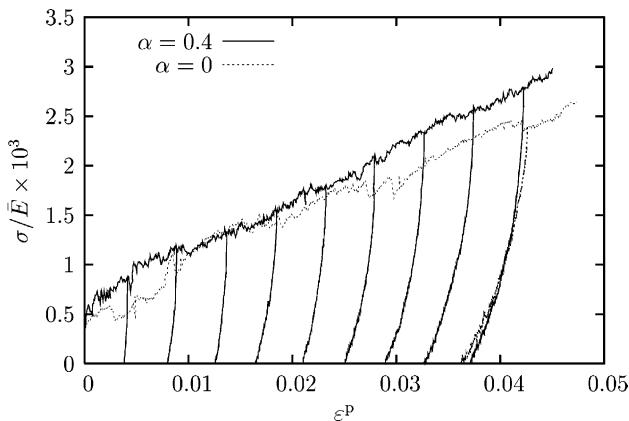

Fig. 6. Stress, σ, normalized by the plane strain tensile modulus, $\bar{E}$, versus plastic strain, ε^p, for crystal A in tension and with unloading to $\sigma = 0$ from several strain levels (slip is initially symmetric). For clarity only one unloading curve is shown for $\alpha = 0$.
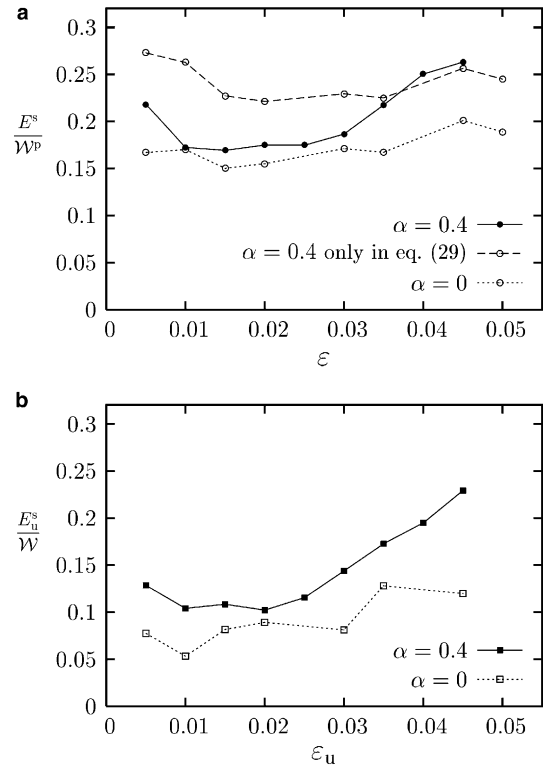

Fig. 7. Evolution of the energy storage with strain for crystal A. (a) Ratio of stored energy, E^s, to plastic work, $\mathscr{W}^p$, versus imposed strain, ε. For the curve marked $\alpha = 0.4$ only in Eq. (29), the line tension does not affect the dislocation dynamics but is accounted for in calculating the stored energy. (b) Ratio of stored energy after unloading, E_u^s, to the total work of deformation, $\mathscr{W}$, versus strain at the beginning of unloading, ε_u.

The rate of change of $E^s/\mathscr{W}^p$ is related to $\dot{E}^s/\dot{\mathscr{W}}^p$ by

$$\frac{d}{dt}\left(\frac{E^s}{\mathscr{W}^p}\right) = \frac{\dot{\mathscr{W}}^p}{\mathscr{W}^p}\left(\frac{\dot{E}^s}{\dot{\mathscr{W}}^p} - \frac{E^s}{\mathscr{W}^p}\right) \tag{24}$$

so that $E^s/\mathscr{W}^p$ is increasing when $E^s/\mathscr{W}^p$ is smaller than $\dot{E}^s/\dot{\mathscr{W}}^p$. On the other hand, from Eq. (7), the incremental storage ratio is

$$\frac{\dot{\Phi}}{\dot{\mathscr{W}}} = \frac{\dot{\Phi}}{\dot{\Phi} + \dot{\mathscr{D}}} \tag{25}$$

so that, if over some interval of applied strain, $\mathscr{D}$ increases more than $\dot{\Phi}$, $\dot{\Phi}/\dot{\mathscr{W}}$ can decrease. For crystal B the incremental storage ratio decreases with increasing strain.

4.3. Energy release and long-range stresses

Fig. 8 shows the evolution of the ratio E_u^s/E^s, which is a measure of the stored energy recovered on unloading, with pre-strain for all three crystals. The results shown for crystal A have $\alpha = 0$ in both Eqs. (5) and (29). For crystal C, where unloading is nearly elastic, E_u^s/E^s is near unity for all pre-strain levels. For crystals A and B, the dislocation density increases during unloading for a sufficiently large pre-strain, while the stored energy
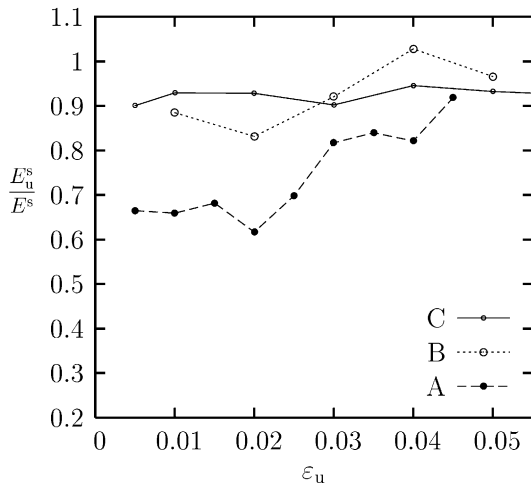
Fig. 8. Ratio of stored energy after load removal and before, E_u^s/E^s, versus strain at the beginning of unloading, ε_u for the three $[\bar{1}10]$ crystals analyzed: crystals C and B with initially unsymmetric slip and crystal A initially symmetric slip. For crystal A and crystal B dynamic obstacles can only be destroyed if the obstacle strength is attained while for crystal C dynamic obstacles also can be destroyed by annihilation of one of the dislocations forming the junction.

decreases. There is a significant Bauschinger effect (see Figs. 4 and 6) and the ratio E_u^s/E^s increases with pre-strain. The recovery ratio, $1 - E_u^s/E^s$, is larger at small strains with the fraction of released energy ranging between $\approx 10\%$ and $\approx 35\%$. For example, for crystal A, E_u^s/E^s increases from 0.67 at $\varepsilon_u = 0.01$ up to 0.9 at $\varepsilon_u = 0.05$. For crystal B, E_u^s/E^s slightly exceeds unity for $\varepsilon_u = 0.04$ so that the stored energy in the unloaded state is greater than the stored energy under load.

The energy release predicted here is consistent with available experimental results [21] as is the increase in dislocation density after load reversal [22]. It is also worth noting that the decrease in stored energy on unloading together with the increase in dislocation density on unloading indicates that the dislocation density does not completely characterize the state of the material because both a strain increase and a strain decrease can give rise to the same value of the dislocation density, but with different internal stress states.

Part of the energy stored in the dislocation structure is due to the long-range stresses associated with that structure. Hence, the question arises as to what extent the short-range stress fields of the dislocation structure contribute to the internal energy. Calculations of the stored energy were carried out for representative states of both crystals A and B where each dislocation in the distribution was replaced by a dipole that only had a short-range $1/r^2$ field. For these calculations, the image field contributions were updated according to the
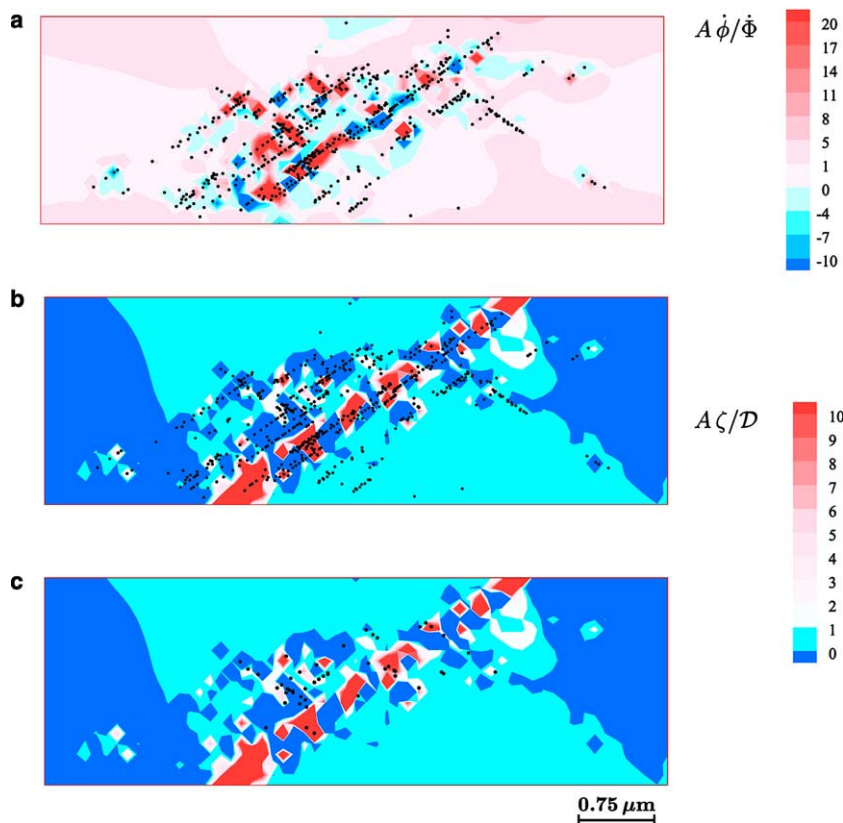

Fig. 9. Distributions at $\varepsilon = 0.01$ of (a) the local stored energy rate $\dot{\phi}$, and (b) the local plastic dissipation ζ, in crystal B. Both local variables are normalized with their respective global quantities per unit of specimen area A. Slip is initially unsymmetric. (c) Local dissipation rate ζ with the current locations of dynamic junctions superposed.

Fig. 10. Distributions at $\varepsilon = 0.04$ of (a) the local stored energy rate $\dot{\phi}$, and (b) the local plastic dissipation ζ, in crystal B. Both local variables are normalized with their respective global quantities per unit of specimen area A. Slip is initially unsymmetric. (c) Local dissipation rate ζ with the current locations of dynamic junctions superposed.
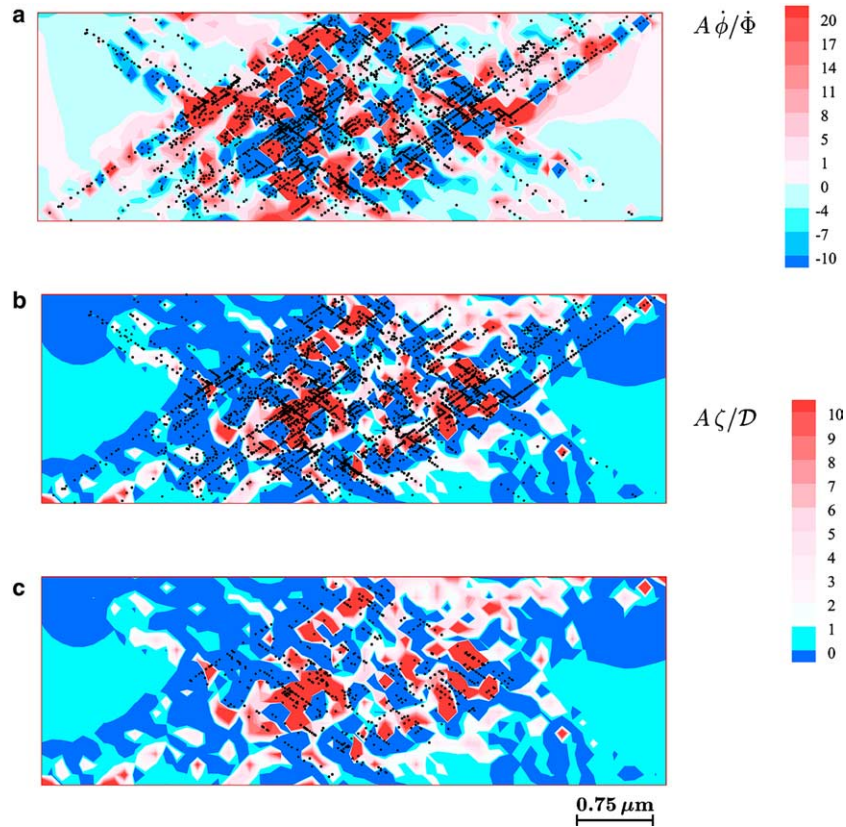
dipolar configuration. In all cases analyzed, including states with high dislocation densities, the stored energy with the long-range fields removed was found to be less than 5% of the stored energy with the long-range fields accounted for. Hence, up to the strains reached in the simulations, most of the energy stored in the dislocations is associated with their long-range fields.

In an attempt to better characterize the cold-worked state of the material, several states having the same dislocation density but different values of the stored energy were analyzed. One such example for crystal A corresponds to a pre-strain of $\varepsilon_u = 0.02$ where the dislocation density is nearly the same in the loaded and unloaded states and equal to $1.5 \times 10^{14}\,\mathrm{m}^{-2}$. The unloaded state has a stored energy about 40% smaller than the loaded state (see Fig. 8). The stored energy associated with the short-range fields is approximately the same in both the loaded and unloaded states, but the two states have different long-range fields. Thus, when long-range stresses are present the dislocation density does not characterize the state of the material.

4.4. Distributions of stored energy and dissipation

The temperature rise during an adiabatic process is known to be heterogeneous and so are processes such as recovery and recrystallization. The spatial fluctuations of the stored energy are therefore worth investigating. Figs. 9 and 10 show spatial distributions of the rate of change of stored energy, $\dot{\phi}$, and of the dissipation, ζ, in crystal B at $\varepsilon = 0.01$ and $\varepsilon = 0.04$, respectively. The contribution of the core energy term, E_1^s in Eq. (11), is not included in $\dot{\phi}$. The values of $\dot{\phi}$ and ζ are normalized by the corresponding global values $\dot{\Phi}/A$ and $\mathscr{D}/A$. The current dislocation distributions are shown in Figs. 9 and 10(a) and (b) while the locations of the dynamic junctions are shown in Figs. 9(c) and 10(c). Since the energy values are computed as element averages via Eq. (21), the values of $\dot{\phi}$ and ζ represent averages over a small area. Such averages are thus defined over a length scale that is much smaller than that of the long-range stresses, which dominate the stored energy. While both the stored energy and the dissipation are nonuniformly distributed over the sample, the dissipation is more localized, particularly during stage I deformation ($\varepsilon = 0.01$). Large variations in $\dot{\phi}$ are seen in regions with high dislocation density (Fig. 9(a)) but regions with high dissipation rate are not necessarily densely populated with dislocations (Fig. 9(b)). At $\varepsilon = 0.01$, the dissipation is localized in an inclined band where glide is occurring.

Although the rate of change of global stored energy $\dot{\Phi}$ is positive at both strain levels, there are regions in the
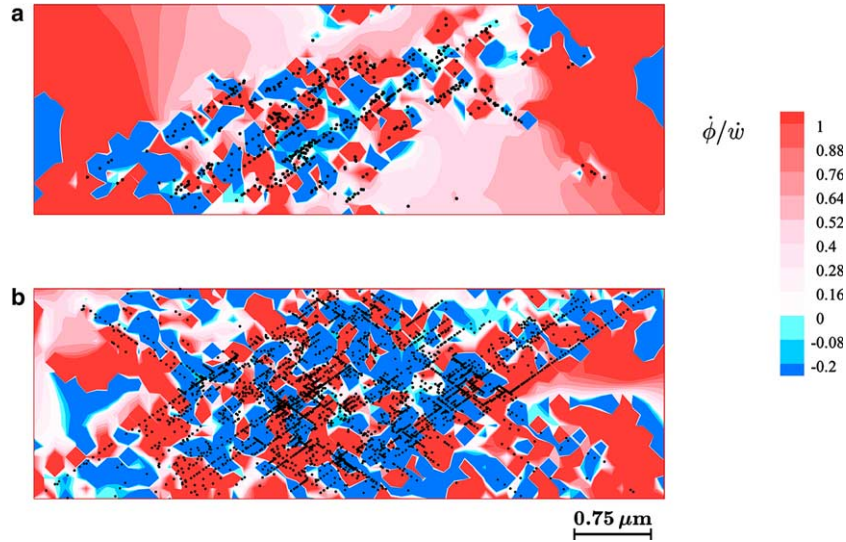
Fig. 11. Distributions of the ratio of the local stored energy rate, $\dot{\phi}$, to the local rate of working, $\dot{w}$, in crystal B. Slip is initially unsymmetric. (a) $\varepsilon = 0.01$. (b) $\varepsilon = 0.04$.

crystal where the rate of change of the local stored energy decreases, $\dot{\phi}/\dot{\Phi} < 0$. The size of the regions with $\dot{\phi} < 0$ increases with increasing straining. In these regions, which have high dislocation densities, dynamic recovery processes take place as early as in stage I ($\varepsilon = 0.01$) and become prominent in well-developed stage II ($\varepsilon = 0.04$). The incremental storage ratio, $\dot{\Phi}/\dot{\mathcal{W}}$, decreases from 0.27 at $\varepsilon = 0.01$ down to 0.17 at $\varepsilon = 0.04$. However, the rate of energy storage $\dot{E}^s/\dot{\mathcal{W}}^p$ (with $\dot{E}^s = \dot{\Phi} - \dot{\mathcal{W}}^e$) is found to increase from 0.045 at $\varepsilon = 0.01$ up to 0.23 at $\varepsilon = 0.04$, which is similar to the trend seen in Fig. 5(a) for $E^s/\mathcal{W}^p$. The ratio $\dot{E}^s/\dot{\mathcal{W}}^p$ was found to be larger than the ratio $E^s/\mathcal{W}^p$ for $0.01 \leqslant \varepsilon \leqslant 0.04$, consistent with the steady increase of $E^s/\mathcal{W}^p$ over that strain range as predicted by Eq. (24).

Fig. 11 shows the distribution of the rate of energy storage, $\dot{\phi}/\dot{w}$, and the dislocation positions at both $\varepsilon = 0.01$ and $\varepsilon = 0.04$, where $\dot{w}$ is defined in Eq. (21). In regions that remain elastic, $\dot{\phi}/\dot{w}$ is about unity as expected[1] but even in regions with a high dislocation density this ratio has peak values much higher than the overall ratio, $\dot{\Phi}/\dot{\mathcal{W}}$. As a consequence, the fraction of work dissipated can be as low as 30–50% over regions of significant size. Hence, local values of the energy storage rate can differ significantly from global values.

4.5. Symmetric versus unsymmetric slip

Fig. 12 shows a comparison between calculations with initially symmetric and initially unsymmetric slip for crystal B. As seen in Fig. 12(a) for the calculation with

---

[1] The values of $\dot{\phi}/\dot{w}$ differing significantly from unity in the regions near the boundaries where displacements are prescribed are a numerical artifact associated with extrapolating ratios of small numbers.
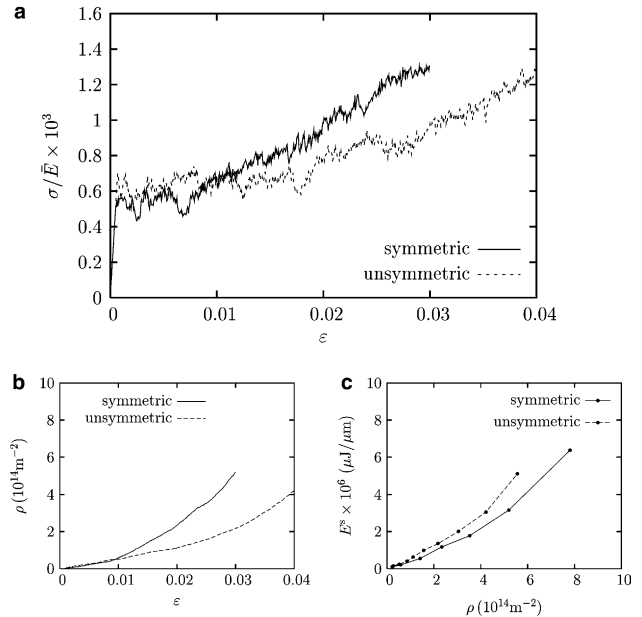

Fig. 12. Initially symmetric versus unsymmetric slip for crystal B. (a) Stress, σ, normalized by the plane strain tensile modulus, $\bar{E}$, versus imposed strain, ε. (b) Dislocation density, ρ, versus imposed strain, ε. (c) Stored energy, E^s, per μm thickness, versus dislocation density, ρ.

initially symmetric slip, stage I is almost, but not completely, suppressed because the low probability of forming junctions at small strains permits some easy glide. However, the stage II hardening rate is nearly the same in both calculations. In addition, for both the calculations with initially unsymmetric slip and with initially symmetric slip, the evolution of the dislocation density ρ remains the same up to a strain of about 0.008, but then ρ is greater for the calculation with initially symmetric slip, Fig. 12(b). A cross plot of the data in Figs. 12(a)

and (b) (not shown) to give σ as a function of dislocation density ρ shows that the curves for the initially symmetric and initially unsymmetric slip calculations coincide because the flow strength scales with $\sqrt{\rho}$, see Eq. (22).

When the stored energy E^s is plotted against the strain ε then E^s at a given value of ε is greater for initially symmetric slip. On the other hand, when E^s is plotted against the dislocation density ρ, Fig. 12(c), the stored energy with initially symmetric slip is less than that with initially unsymmetric slip, for a sufficiently large value of ρ. Therefore, the stored energy depends on the dislocation structure that forms, not just on the dislocation density.

4.6. Effect of crystal orientation

The two orientations sketched in Fig. 1 are investigated using the data for crystal B. The calculated stress–strain response of the [0 0 1] crystal is compared with that of the [$\bar{1}$ 1 0] crystal in Fig. 13(a). Within the strain interval of the simulations, the rate of linear stage II hardening is essentially the same for both orientations, but with a tendency for stage II to set in earlier in the [0 0 1] crystal. Although the latter effect is small, it is consistent with published results on the effect of crystal orientation on the extent of stage I hardening; see e.g. [23].

Also, the rate of increase of the dislocation density is greater in the [0 0 1] crystal than in the [$\bar{1}$ 1 0] crystal, Fig. 13(b). This is due to the combined effect of a larger number of active slip planes and a larger value of the density of static sources in the [0 0 1] crystal (ρ_0 for the [0 0 1] crystal is about twice its value for the [$\bar{1}$ 1 0] crystal). Because of the geometry there are more slip planes in the [0 0 1] crystal for fixed crystal dimensions and slip plane spacing, which increases the probability for junction formation. Thus, the accumulated density of dynamic dislocation sources is also found to be larger in the [0 0 1] crystal. The dislocation density, ρ, normalized by the initial source density ρ_0 is a measure of the average dislocation density per slip plane (the number of static sources per slip plane is the same for both orientations). If ρ/ρ_0 is plotted against the applied strain then the trend seen for the total dislocation density is reversed for the average dislocation density per slip plane, with ρ/ρ_0 being smaller in the [0 0 1] crystal. These same trends are observed for the mobile dislocation densities.

Interestingly, the difference between the two crystal orientations in terms of the stored energy E^s, Fig. 13(c), shows that there is no simple scaling between E^s and the dislocation density. The stored energy in the [0 0 1] crystal is smaller than in the [$\bar{1}$ 1 0] crystal at a given dislocation density. These results, together with those in Fig. 12(c), indicate that the energy stored in the crystal is affected by the higher order moments of the dislocation pattern whereas the flow stress and the work hardening rate are not. Both the geometry of slip and the development of a dislocation structure during stage II play important roles in determining the features of the dislocation distribution that affect the energy storage.
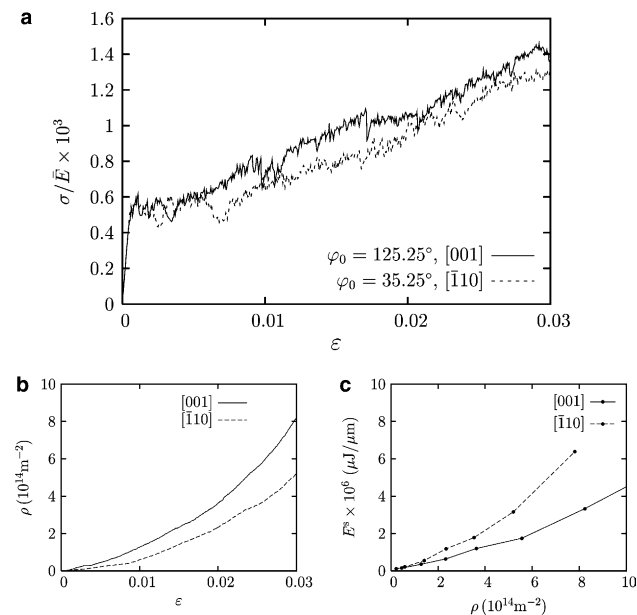
5. Discussion

The parameters characterizing the three crystals considered are chosen so that a variety of responses are obtained over the range of strain covered in the calculations (up to 0.1). The work hardening rate of crystal C is representative of some ductile metal crystals ($\approx 2 \times 10^{-3}\mu$ where μ is the elastic shear modulus). The parameters characterizing crystals A and B give rise to increased dislocation storage over the strain levels analyzed, leading to a hardening rate about an order of magnitude larger than for crystal C, but this permits responses to be explored that would require calculations to much larger strains with a lower work hardening rate.

The calculations here are purely mechanical with any entropy contribution to the free energy ignored. Cottrell [19] has estimated the entropy contribution to the free energy in a dislocated crystal and concluded that at low temperatures, this entropy contribution is small so that the elastic energy can be identified with the free energy. The elastic energy stored is directly associated with the evolution of the dislocation structure. As discussed in [15], the key to the development of a dislocation structure in these simulations is accounting for dynamic junc-

Fig. 13. Effect of crystal orientation using the parameter values for crystal B. (a) Stress, σ, normalized by the plane strain tensile modulus, $\bar{E}$, versus imposed strain, ε. (b) Dislocation density, ρ, versus imposed strain, ε. (c) Stored energy, E^s, per μm thickness, versus dislocation density, ρ.

tion formation. This is clearly seen in Fig. 5 where the stored energy evolution for calculations with and without the formation of dynamic junctions are compared. On the other hand, although accounting for line tension does not qualitatively affect the predicted behavior, except at very small strains, there can be a significant quantitative contribution (Figs. 5 and 7). An additive contribution of line tension to the free energy similar to that in Eq. (11) has been adopted by several authors; see e.g. [24] and references therein.

The ratio of the stored energy associated with the internal stress state, E_u^s, to the total expended work, $\mathscr{W}$, is appropriate for comparisons with most experimental results in the review by Bever et al. [1] and, e.g., in [4], whereas the ratio of the stored energy under load, E^s, to the plastic work, $\mathscr{W}^p$, may be more appropriate for comparison with the data in [6,10] where the stress and the temperature rise, which is related to the dissipation, were measured and then, assuming an adiabatic process, the energy storage inferred. The values calculated here for both $E_u^s/\mathscr{W}$ and $E^s/\mathscr{W}^p$ are between 0.04 and 0.30, which is a representative range for values measured in tension [1]. The evolution of the storage ratio with strain varies significantly for the three crystals considered. Similarly, a wide range of behaviors is seen experimentally. Bever et al. [1] show behavior similar to that obtained here for crystal B in their Fig. 28 (based on data from Williams [25]). An evolution of $E^s/\mathscr{W}^p$ qualitatively similar to that for crystal A was measured by Rosakis et al. [10] for α-titanium (their Fig. 8). Note that in Fig. 7(a) there is a strain range with little variation of $E^s/\mathscr{W}^p$ with strain, which suggests that $\dot{E}^s/\dot{\mathscr{W}}^p \approx E^s/\mathscr{W}^p$ by virtue of Eq. (24), and then $E^s/\mathscr{W}^p$ increases at larger strains. The curve of $E^s/\mathscr{W}^p$ versus strain in Fig. 7(a) is consistent with the existence of a maximum in the overall $E^s/\mathscr{W}^p$ versus strain curve, first noticed in [25] and later also seen in [2,3].

Interestingly, Rosakis et al. [10] also report that, for polycrystalline aluminum, the percentage of plastic work dissipated in heating is only between 25% and 60% of the total plastic work up to a strain of 0.15. Thus, in [10] the stored energy is a much greater fraction of the work of deformation than in most other investigations. As noted in discussing the energy plots in Figs. 9–11, the dissipation caused by plastic deformation, and therefore the temperature rise, can be very localized. Hence, it is possible that the dissipation values in [10], which were inferred by measuring an area-averaged temperature rise, underestimate the energy dissipation. On the other hand, in [6] values of the ratio of plastic work dissipated in heating to total plastic work up to 0.95 were reported for strains above 0.3 so that another possibility is that the behavior reported in [10] pertains to a small strain regime ($\varepsilon < 0.3$) involving a dislocation structure with substantial long range stresses.

The calculations in this study were carried out at a relatively high strain rate (of the order of 10^2 s^{-1}) to lim-

it the computation time, with the dislocation constitutive parameters chosen to represent behavior in the relatively rate independent quasi-static loading regime. The effect of strain rate on the evolution of the stored energy is not explored here. Indeed, there are only limited experimental studies of the effect of strain rate on the stored energy. Those reported in the review by Bever et al. [1, pp. 56–59] and in Hodowany et al. [6] suggest that the effect of strain rate may vary with the material and is not necessarily monotonic for a given material.

The dependence of the stored energy on dislocation density is summarized in Fig. 14 for all three crystals A, B and C (the results do not include the line energy). In order to facilitate comparison with the experimental data in [4], energies are here given per unit mass using the mass density of aluminum (2700 kg/m^3). The value of the stored energy corresponding to the highest dislocation density attained in crystal B, which is 8×10^{14} m^{-2}, is in good quantitative agreement with that measured by Verdier et al. [4] at the same dislocation density (see their Fig. 5) but at a measured strain level one order of magnitude higher than in crystal B. Thus, the calculations with a high work-hardening rate permit a regime with relatively large dislocation densities to be investigated.

The calculations clearly show that the stored energy is not simply a function of a single parameter, the dislocation density. Furthermore, there is no simple relationship between work-hardening rate and energy storage. The energy stored in crystal C is higher at any given dislocation density than in crystal B although crystal B has a higher hardening rate. This may be a consequence of stronger dislocation interactions in crystal C due to
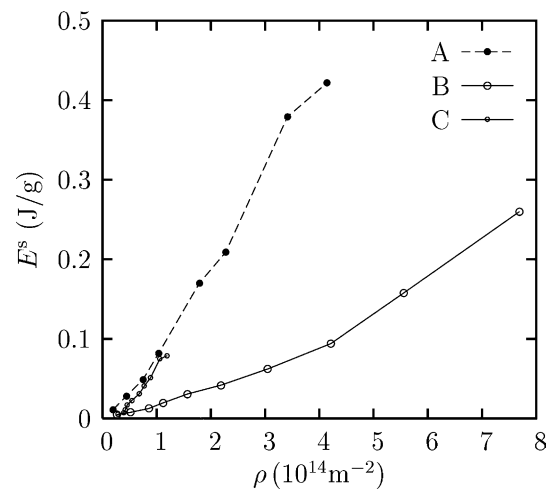

Fig. 14. Energy stored per unit mass versus dislocation density for the three $[\bar{1}10]$ crystals analyzed: crystals C and B with initially unsymmetric slip and crystal A with initially symmetric slip. In all cases $\alpha = 0$. For crystal A and crystal B dynamic obstacles can only be destroyed if the obstacle strength is attained while for crystal C dynamic obstacles also can be destroyed by annihilation of one of the dislocations forming the junction.

the smaller spacing between active slip planes. More generally, the elastic energy associated with a dislocation density strongly depends on how the dislocations are arranged in the material. Thus, at a given dislocation density, the stored energy can vary with material, for example the energy per unit dislocation length E^s/ρ is found to be smaller in crystal B than in crystal A and, for a given material, can vary with the imposed loading history (stress state, loading rate, etc.).

Since the stored energy is associated with an internal stress state, it is not surprising that there is a correlation between E^s and the Bauschinger effect. Such a correlation is seen in the results obtained here. For crystal C, where $E^s/\mathscr{W}^p$ is less than 0.05, unloading is nearly elastic, while for crystal B, the Bauschinger effect increases with increasing strain and there is a particularly rapid increase in the later stages of deformation calculated. For crystal A, a similar Bauschinger effect is seen for the last three unloading curves (the curves are approximately parallel) consistent with the nearly constant value of $E^s/\mathscr{W}^p$.

The extent to which the stored energy depends on the boundary conditions was explored by explicitly calculating the contribution of the image forces. With $E^s_{\text{no img}}$ denoting the stored energy computed with the image field contribution in Eq. (11) neglected, we calculated $(E^s - E^s_{\text{no img}})/E^s$ at various strain levels for all three crystals, both in the loaded and unloaded states. The value of $(E^s - E^s_{\text{no img}})/E^s$ varied between $\approx +1.2$ and ≈ -1.2, with the smallest values for crystal C (between -0.2 and $+0.2$ for $\varepsilon > 0.04$). Crystal C has the lowest ratio of stored energy to plastic work and does not exhibit a Bauschinger effect. This suggests that when the energy of the dislocation structure is low, either due to a low density of dislocations or a well-shielded dislocation structure, the image contribution is small. However, when there are dislocation structures with a relatively high internal energy (say 5% or more of the plastic work as for crystals A and B), the image force contribution can be substantial.

The evolution of the energy storage is of interest in the formulation of continuum models of plastic deformation. The dissipation associated with plastic deformation can induce a significant temperature rise and an input to thermo-plasticity calculations is the fraction of plastic work converted to heat. This is typically taken to be a constant equal to 0.9, as indicated by the experiments of Taylor and Quinney [26]. Consistent with the preponderance of experimental data, the calculations suggest that assuming a constant value of 0.9 could lead to an incorrect prediction of the temperature rise, at least over the range of straining considered here. In calculations based on phenomenological plasticity theories, the fraction of plastic work converted into heat is generally taken to be independent of the stress state induced by the imposed loading. The sensitivity of the ratio $E^s/\mathscr{W}^p$ to the dislocation structure formed suggests that this assumption is not valid.

6. Conclusions

Discrete dislocation plasticity analyses of the energy stored and dissipated have been carried out for planar single crystals subject to tension. Although the calculations are two-dimensional, constitutive rules that incorporate aspects of the physics of three-dimensional dislocation interactions [15] have been used. As a consequence, the dislocation density increases with increasing deformation and it is the elastic energy associated with the dislocation structures that represents the stored energy of cold work.

- The predictions of the energy stored and dissipated are consistent with published experimental results regarding the magnitude and evolution of the ratio of energy stored to the work of deformation, the decrease of the incremental rate of energy storage for sufficient strain and the partial energy release on loading reversal.
- Although the flow stress and work hardening rate depend mainly on the dislocation density, the stored energy of cold work depends on details of the dislocation structure that forms.
  - The dislocation density does not fully characterize the state of the material because a given dislocation density can correspond to different internal stress states.
  - The formation of dislocation patterns with long-range stress fields increases the energy storage and dislocation patterns that enhance dislocation screening reduce the energy storage.
- Even in a state of macroscopically "homogeneous" tension, local values of the energy storage and dissipation can differ significantly from global values.
- There is a connection between the stored energy of cold work and the Bauschinger effect.
- Discrete dislocation plasticity provides a framework for investigating the role of material and loading parameters that affect the fraction of plastic work converted to heat.

Appendix

The line energy term in Eq. (11) is defined by

$$E^s_1 = \sum_i \left[\frac{1}{2} \int_{\hat{V}^i} \boldsymbol{\sigma}^i : \boldsymbol{\varepsilon}^i \, dV + \frac{1}{2} \int_{C^i} \mathbf{t}^i \cdot \mathbf{u}^i \, dS \right] + E^i_c. \qquad (26)$$

Here, E_l^s, is calculated assuming a statistically homogeneous distribution of dislocation loops across the thickness of the strip. Thus, per unit thickness

$$E_l^s = \sum_i \frac{1}{\mathscr{S}^i} \int_{\mathscr{C}^i} \mathscr{E} \, dl, \tag{27}$$

where the summation is on loops in the plane of analysis, $\mathscr{S}^i$ refers to the out-of-plane loop spacing averaged over a "row" of loops, $\mathscr{C}^i$ is the dislocation line and $\mathscr{E}$ is the line energy per unit length, which is taken to be independent of position around the dislocation loop and equal to $\alpha\mu b^2$ [17,15] with α the same factor used in Eq. (5).

In plane strain, the dislocation loops will expand in the plane of deformation much more than out of plane and we neglect the out-of-plane loop size. This assumption is further justified by the fact that edge segments move faster than screws and, in the configuration considered here, the out-of-plane segments would be screws. Hence, assuming a prismatic shape, the line integral in Eq. (27) is $2\mathscr{S}_d^i\mathscr{E}$ where $\mathscr{S}_d^i$ is the in-plane loop size (the factor two arises because the dislocation loop has two segments of length $\mathscr{S}_d^i$). The line energy is then given by

$$E_l^s = \sum_i 2\frac{\mathscr{S}_d^i}{\mathscr{S}^i}\mathscr{E}. \tag{28}$$

The value of E_l^s thus depends on the ratio of the in-plane loop size to the out-of-plane loop spacing. For simplicity we take $\mathscr{S}_d^i/\mathscr{S}^i = 1$ and E_l^s is then $2N_p\mathscr{E} = 2N_p\alpha\mu b^2$ where N_p is the number of paired dislocations (including dislocation–exit point pairs) in the plane of analysis. Note that any deviation of $\mathscr{S}_d^i/\mathscr{S}^i$ from unity can be incorporated into the value of the line tension coefficient α.

Among the N_p pairs there are N' dislocations coupled with a step representing half-loops and N'' pairs of coupled dislocations (i.e., dipoles) representing full loops; thus, $N_p = N' + N''$ and the total number of dislocations is $N = N' + 2N''$. This gives the number of pairs in Eq. (27) as $N_p = (N + N')/2$ and the line tension per unit thickness then becomes

$$E_l^s = 2N_p\mathscr{E} = (\rho + \rho')A\alpha\mu b^2, \tag{29}$$

where $A = (2h)(2l)$ is the area of the specimen, ρ is the dislocation density and ρ' is the density of dislocations coupled with a step. A nonzero value of ρ' indicates a non zero net Burgers vector. To compute E_l^s at any increment, one must keep track of partners in dipoles in order to determine ρ'.

References

[1] Bever MB, Holt DL, Titchener AL. Prog Mater Sci 1973;17:1–190.

[2] Mason JJ, Rosakis AJ, Ravichandran G. Mech Mater 1994;17:135–45.

[3] Oliferuk W, Korbel A, Grabski MW. Mater Sci Eng A 1996;220:123–8.

[4] Verdier M, Groma I, Flandin L, Lendvai J, Bréchet Y, Guyot P. Scripta Mater 1997;37:449–54.

[5] Kapoor R, Nemat-Nasser S. Mech Mater 1998;27:1–12.

[6] Hodowany J, Ravichandran G, Rosakis AJ, Rosakis P. Exp Mech 2000;40:113–23.

[7] Rice JR. J Mech Phys Solids 1971;19:433–55.

[8] Germain P, Nguyen QS, Suquet P. J App Mech 1983;50:1010–20.

[9] Chaboche J-L. J App Mech 1993;60:822–8.

[10] Rosakis P, Rosakis AJ, Ravichandran G, Hodowany J. J Mech Phys Solids 2000;48:581–607.

[11] Aravas N, Kim K-S, Leckie FA. J Eng Mat Tech 1990;112:465–70.

[12] Mollica F, Rajagopal KR, Srinivasa AR. Int J Plasticity 2001;17:1119–46.

[13] Van der Giessen E, Needleman A. Modelling Simul Mater Sci Eng 1995;3:689–735.

[14] Weygand D, Friedman LH, Van der Giessen E, Needleman A. Modelling Simul Mater Sci Eng 2002;10:437–68.

[15] Benzerga AA, Bréchet Y, Needleman A, Van der Giessen E. Modelling Simul Mater Sci Eng 2004;12:159–96.

[16] Hirth JP, Lothe J. Theory of dislocations. New York: McGraw-Hill; 1968.

[17] Kuhlmann-Wilsdorf D. Mater Sci Eng 1970;A113:1–41.

[18] Lubarda V, Blume JA, Needleman A. Acta Metall Mater 1993;41:625–42.

[19] Cottrell AH. Dislocations and plastic flow in crystals. Oxford: Clarendon Press; 1953.

[20] Friedel J. Les dislocations. Paris: Gauthier-Villars; 1956.

[21] Iyer AS, Gordon P. Trans Met Soc AIME 1959;215:729–30.

[22] Hasegawa T, Yakou T, Karashima S. Mater Sci Eng 1975;20:267–76.

[23] Diehl J, Mader S, Seeger A. Z Metallkd 1955;46:650–7.

[24] Ortiz M, Repetto EA. J Mech Phys Solids 1999;47:397–462.

[25] Williams RO. Acta Metall 1964;12:745–7.

[26] Taylor GI, Quinney H. Proc Roy Soc London A 1934;A143:307–26.